

ARTICLE

Open Access

Inhibition of glioblastoma cell proliferation, invasion, and mechanism of action of a novel hydroxamic acid hybrid molecule

Issan Zhang¹, Maja Beus^{1,2}, Ursula Stochaj³, Phuong Uyen Le⁴, Branka Zorc², Zrinka Rajić², Kevin Petrecca⁴ and Dusica Maysinger¹

Abstract

Glioblastoma multiforme is one of the most aggressive brain tumors and current therapies with temozolomide or suberoylanilide hydroxamic acid (SAHA, vorinostat) show considerable limitations. SAHA is a histone deacetylase (HDAC) inhibitor that can cause undesirable side effects due to the lack of selectivity. We show here properties of a novel hybrid molecule, sahaquine, which selectively inhibits cytoplasmic HDAC6 at nanomolar concentrations without markedly suppressing class I HDACs. Inhibition of HDAC6 leads to significant α -tubulin acetylation, thereby impairing cytoskeletal organization in glioblastoma cells. The primaquine moiety of sahaquine reduced the activity of P-glycoprotein, which contributes to glioblastoma multiforme drug resistance. We propose the mechanism of action of sahaquine to implicate HDAC6 inhibition together with suppression of epidermal growth factor receptor and downstream kinase activity, which are prominent therapeutic targets in glioblastoma multiforme. Sahaquine significantly reduces the viability and invasiveness of glioblastoma tumoroids, as well as brain tumor stem cells, which are key to tumor survival and recurrence. These effects are augmented with the combination of sahaquine with temozolomide, the natural compound quercetin or buthionine sulfoximine, an inhibitor of glutathione biosynthesis. Thus, a combination of agents disrupting glioblastoma and brain tumor stem cell homeostasis provides an effective anti-cancer intervention.

Introduction

Glioblastoma multiforme (GBM) is the most common and aggressive form of brain cancer, with limited treatment options and dismal survival rates. Current treatment involves surgical resection followed by radiotherapy and chemotherapy with temozolomide (TMZ)¹. However, more than half of GBM patients do not respond to TMZ due to the overexpression of DNA repair enzymes, notably *O*⁶-methylguanine transferase^{2–4}.

Histone deacetylase (HDAC) inhibitors exert anticancer effects by inducing cell differentiation, cell cycle arrest, and apoptotic cell death through the upregulation of tumor suppressor and cell cycle-regulatory genes⁵. Suberoylanilide hydroxamic acid (SAHA, vorinostat) is a Food and Drug Administration-approved drug for the treatment of cutaneous T cell lymphoma. It is currently in clinical trials for GBM as monotherapy and combined with radiotherapy^{6–9}. Despite advancements in treatments, the median survival rate for GBM remains low (14–16 months) and new therapeutic options are urgently needed^{3,10}.

In this study, we combined hydroxamic acid—the active moiety of SAHA exerting biological effects in cancer cells—with primaquine to generate a new class of hybrid anticancer agents: sahaquines. Hydroxamic acid inhibits HDACs;

Correspondence: Dusica Maysinger (dusica.maysinger@mcgill.ca)

¹Department of Pharmacology and Therapeutics, McGill University, Montreal, QC, Canada

²Faculty of Pharmacy and Biochemistry, University of Zagreb, Zagreb, Croatia
Full list of author information is available at the end of the article.

These authors contributed equally: Issan Zhang, Maja Beus

Edited by M.V. Niklison Chirou

© 2018 The Author(s).



Open Access This article is licensed under a Creative Commons Attribution 4.0 International License, which permits use, sharing, adaptation, distribution and reproduction in any medium or format, as long as you give appropriate credit to the original author(s) and the source, provide a link to the Creative Commons license, and indicate if changes were made. The images or other third party material in this article are included in the article's Creative Commons license, unless indicated otherwise in a credit line to the material. If material is not included in the article's Creative Commons license and your intended use is not permitted by statutory regulation or exceeds the permitted use, you will need to obtain permission directly from the copyright holder. To view a copy of this license, visit <http://creativecommons.org/licenses/by/4.0/>.

these enzymes are overexpressed in many cancers, including GBM^{11,12}. The hydroxamic acid pharmacophore of SAHA chelates metal ions, thereby inhibiting metalloenzymes such as HDACs and matrix metalloproteinases (MMPs), which promote cancer growth and invasiveness^{13–15}. Hydroxamic acid is a weak acid, which is favorable in the acidic tumor microenvironment as weak bases become protonated, resulting in ion trapping, lysosomal accumulation, elimination by lysosomal exocytosis, and overall decreased biological activity^{16–18}. Primaquine can directly interfere with endosomal trafficking to the plasma membrane¹⁹, inhibit the multidrug resistance transporter P-glycoprotein, and autophagy, thereby sensitizing cancer cells to anti-mitotic drugs^{20,21}. Considering that monotherapies have limited effectiveness in GBM, we tested sahaquine in combination with TMZ, the standard of care for GBM, quercetin, and buthionine sulfoxamine. Quercetin is an abundant flavonoid found in fruits and vegetables, such as apples and onions. Its estimated daily intake ranges from 3–40 mg, but supplements up to 1000 mg per day are considered safe²². Although it shows no toxicity in normal cells, several studies have shown that quercetin has anticancer effects. Its mechanism of action involves the upregulation of pro-apoptotic and down-regulation of anti-apoptotic factors, cell cycle arrest, and DNA intercalation, resulting in DNA damage, activation of apoptosis, and cell death²³. In animal studies, quercetin inhibited tumor growth and improved the lifespan of tumor-bearing mice^{23,24}. Furthermore, the anticancer effects of quercetin are enhanced in combination with chemotherapeutic agents or other drugs^{25–27}.

We investigated the loss of cell viability and invasiveness in GBM as functional read-outs of the effects of sahaquine alone or in combination with TMZ and quercetin. Sahaquine was tested in both differentiated GBM cells and brain tumor stem cells (BTSCs), which are key to tumor survival

and recurrence^{28–31}. Our study supports the model that sahaquine-induced cell death of GBM is mediated through multiple pathways, including inhibition of HDAC6, reduction of epidermal growth factor receptor (EGFR) protein abundance, and decreased activation of downstream kinases AKT and ERK1/2. The primaquine moiety of sahaquine contributes to the inhibition of P-glycoprotein. Considering that sahaquine significantly reduced BTSC viability and markedly inhibited GBM invasion by disruption of GBM homeostasis, further systematic studies are warranted in patient-derived organoids.

Results

Sahaquine synthesis and physicochemical properties of the selected anticancer agents

Sahaquine is a primaquine and hydroxamic acid derivative linked with glutaric acid. It is synthesized in four steps (Fig. 1). The pharmacophore, hydroxamic acid, was introduced in the last step. Yields were good to excellent (50–88%). Sahaquine was fully characterized by conventional spectroscopic and analytical methods (melting point, IR, MS, ¹H-NMR, ¹³C-NMR), and the data were consistent with the proposed structure (Supplementary Fig. S1). The quinoline ring of sahaquine acts as the capping group and the hydroxamic acid binds zinc. Calculations of physicochemical properties showed that TMZ is a hydrophilic compound ($\log P = -0.28$), whereas sahaquine and particularly quercetin are more lipophilic ($\log P = 0.92$ and 2.16, respectively) (Table 1). The isoelectric point (pI) values of these compounds vary from 2.9 (quercetin) to 9.2 (SAHA)³².

Sahaquine is more potent than TMZ for killing human glioblastoma and BTSCs

The half maximal inhibitory concentration (IC₅₀) value of sahaquine (10 μM) was about threefold lower than that

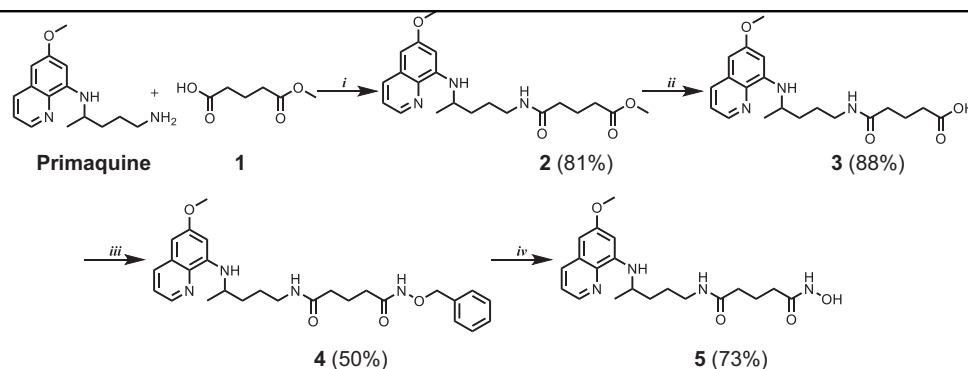
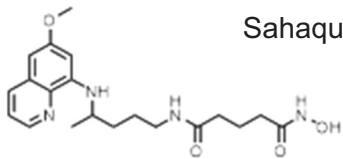
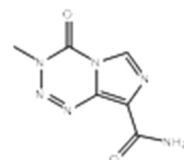
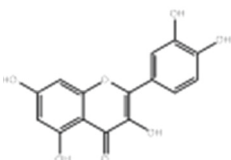
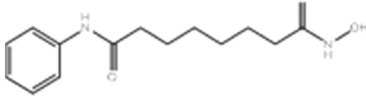


Figure 1 Synthesis of sahaquine and its precursors. Reagents and conditions: (i) HATU, DIEA, dichloromethane, 1 h, (ii) LiOH, methanol, H₂O, 1 h, (iii) O-benzylhydroxylamine, HATU, DIEA, dichloromethane, 2 h, (iv) H₂, 10% Pd/C, methanol, 4 h. All reactions were performed at room temperature. Yields are shown in brackets. HATU 1-[bis(dimethylamino)methylene]-1H-1,2,3-triazolo[4,5-b]pyridinium 3-oxid hexafluorophosphate, DIEA *N,N*-diisopropylethylamine, LiOH lithium hydroxide)

Table 1 Structures of sahaquine, temozolomide, quercetin, and SAHA with basic physicochemical properties

Structure	IUPAC name	Molecular mass	log <i>P</i>	pI
 <p>Sahaquine</p>	<i>N</i> -hydroxy- <i>N'</i> -{4-[(6-methoxyquinolin-8-yl)amino]pentyl}pentanediamide	388.47	0.92	6.48
 <p>Temozolomide</p>	3-methyl-4-oxo-3 <i>H</i> ,4 <i>H</i> -imidazo[4,3- <i>d</i>][1,2,3,5]tetrazine-8-carboxamide	194.15	-0.28	7.1
 <p>Quercetin</p>	2-(3,4-dihydroxyphenyl)-3,5,7-trihydroxy-4 <i>H</i> -chromen-4-one	302.24	2.16	2.9
 <p>SAHA</p>	<i>N'</i> -hydroxy- <i>N</i> -phenyloctanediamide	264.33	1.0	9.2

The physicochemical properties are calculated with the Chemicalize.org program (Instant Cheminformatics Solutions. Available online at <http://www.chemicalize.org/> (accessed on 10 October 2017))

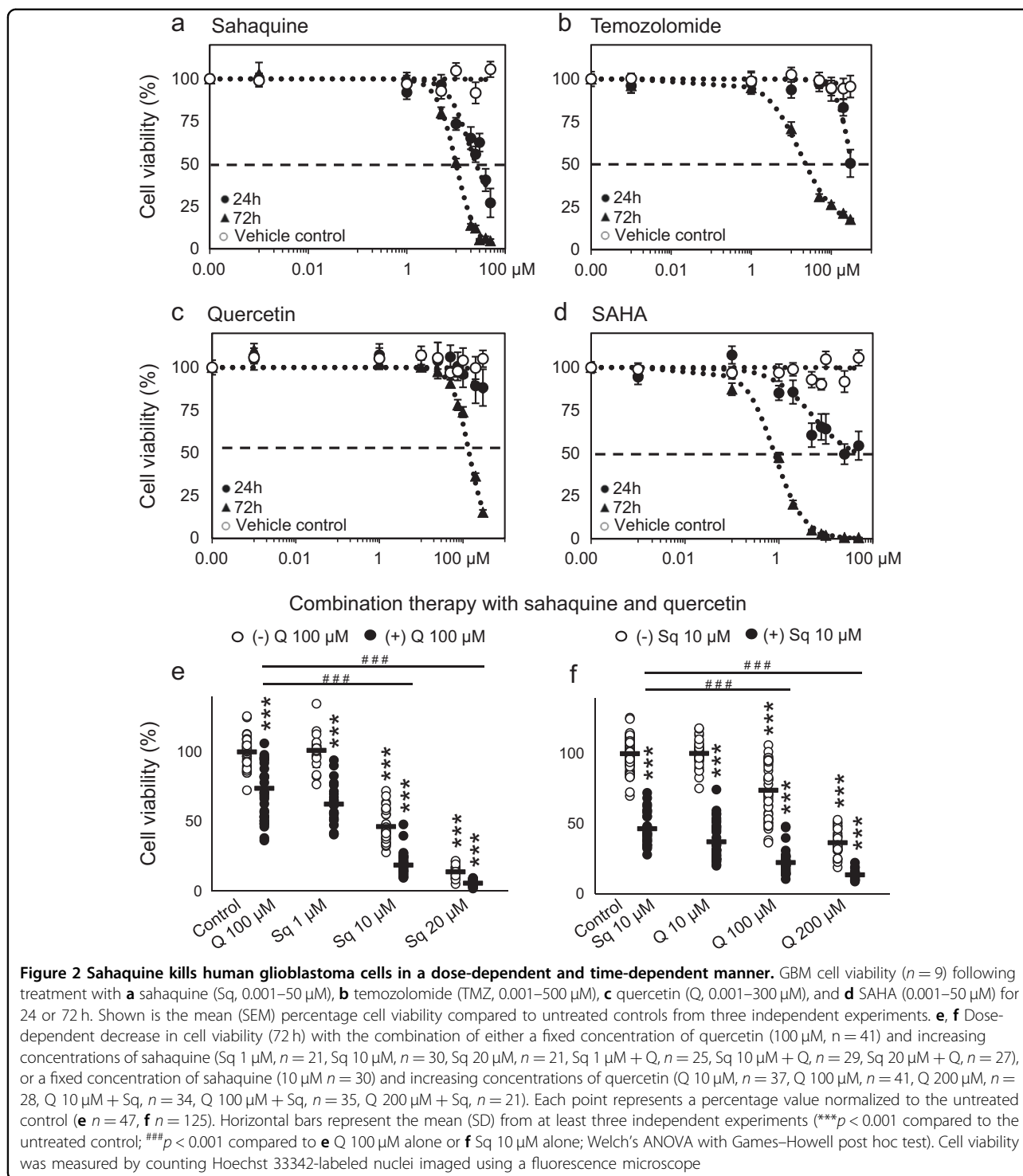
of TMZ (31 μ M), whereas it was less potent than its parent compound SAHA after 72 h incubation (Fig. 2). Sahaquine precursors were also tested, but because of the relatively high IC_{50} values (>50 μ M), further experiments were not pursued (Supplementary Table S1). Enhanced cell killing was achieved by combining quercetin with sahaquine in a dose-dependent manner, although quercetin alone showed limited cytotoxicity (IC_{50} = 140 μ M after 72 h) (Fig. 2e). Combination of TMZ with sahaquine, quercetin, or SAHA at IC_{50} concentrations was more effective than any of the compounds alone (Supplementary Fig. S2). Similar results were obtained by measurements of mitochondrial metabolic activity using the MTT (3-[4,5-dimethylthiazol-2-yl]-2,5-diphenyl tetrazolium bromide) assay (Supplementary Fig. S3).

We further tested the selected compounds on GBM tumoroids, which are more drug-resistant and representative models of brain tumors in vivo. Sahaquine and TMZ reduced tumoroid sizes by 37 and 40%, respectively, while quercetin did not have a significant effect after 7 days (Supplementary Fig. S4).

Based on the results shown in Fig. 2, we investigated the cytotoxic effects of the selected compounds on BTSCs. BTSCs are a key subpopulation of GBM tumors implicated in tumor initiation, propagation and recurrence^{28,30}. In vitro BTSC cultures spontaneously formed neurospheres of approximately 100 μ m in diameter within 7 days. Sahaquine and quercetin were most effective at reducing the size of BTSC aggregates and abolishing the formation of neurospheres (Fig. 3).

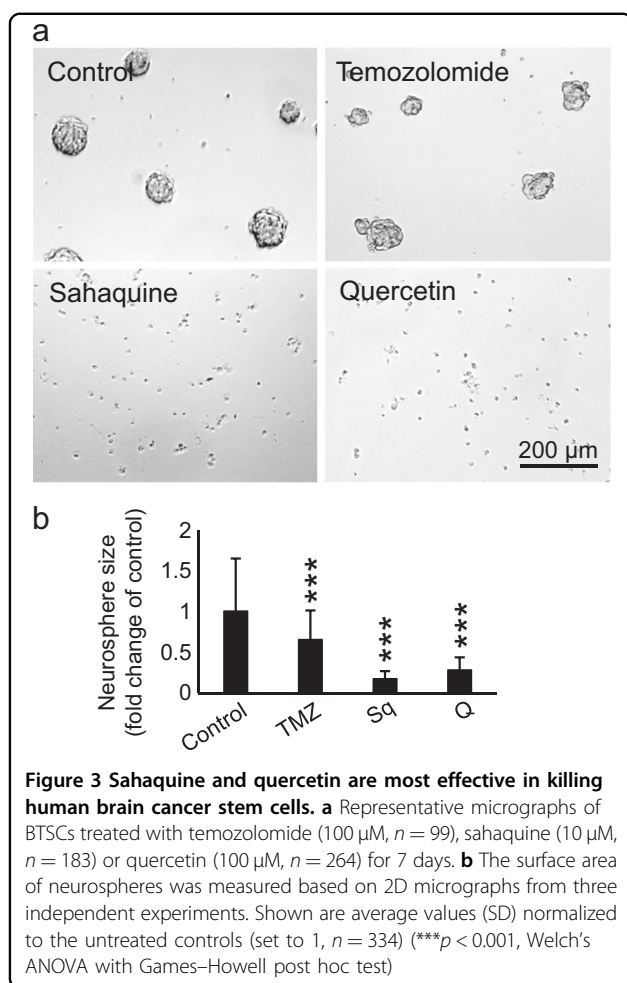
Sahaquine inhibits GBM invasion and P-glycoprotein activity

GBM is characterized by a diffuse brain tissue distribution³³. Tumors commonly reoccur within a few centimeters of the original lesion, making surgical resection difficult³³. We tested the effect of sahaquine and quercetin on GBM migration using a scratch assay, and invasion using a three-dimensional (3D) collagen matrix. Sahaquine did not significantly inhibit cell migration over 24 h, while quercetin reduced cell migration by 20% (Fig. 4a). The combination of sahaquine with quercetin



was most effective, reducing migration by 42%. This effect was not observed when combining sahaquine with TMZ. In contrast, sahaquine significantly inhibited GBM invasiveness, whereas quercetin and TMZ reduced cell invasion by 35 and 45% after 4 days, respectively (Fig. 4c). GBM invasiveness is enabled by MMP degradation of the

extracellular matrix and basement membranes^{34,35}. We investigated the effect of the selected compounds on the abundance of secreted MMPs using gelatin zymography and showed that quercetin decreases MMP abundance in a dose-dependent manner (Supplementary Fig. S5). Neither sahaquine nor TMZ reduced MMP concentrations,



although the hydroxamic acid moiety in sahaquine can bind zinc within the MMP structure³⁶. The primaquine moiety of sahaquine contributed to the inhibition of P-glycoprotein, as assessed by intracellular retention of calcein-AM (Supplementary Fig. S6). The primaquine concentration within sahaquine (10 μ M) effectively inhibited P-glycoprotein activity, whereas 60 μ M of unincorporated primaquine was required to achieve a comparable effect. A smaller extent of P-glycoprotein inhibition by SAHA was obtained with equimolar sahaquine concentrations (10 μ M) (Supplementary Fig. S6).

Sahaquine selectively inhibits HDAC6

We further examined the HDAC inhibitory activity of sahaquine compared to its parent compound SAHA. SAHA is a pan-HDAC inhibitor that caused an increase in both acetylated α -tubulin (K40) and acetylated histone H3 (K9/K14) (Fig. 5). We hypothesized sahaquine to be selective toward HDAC6, because its bulky capping group would fit better into the wide binding site of the enzyme^{37,38}. Nanomolar concentrations (100 nM) of sahaquine resulted in a 1.5-fold increase in acetylated

α -tubulin compared to the untreated control, but did not affect histone acetylation (Fig. 5a). Similar results were obtained with the HDAC6-selective inhibitor ACY-1215 (Supplementary Fig. S7). TMZ and quercetin did not inhibit HDAC6. These results were supported by Western blot analyses (Fig. 5c). HDAC6 abundance was comparable following all treatments, suggesting that sahaquine inhibited the enzyme activity without affecting its protein levels (Fig. 5d).

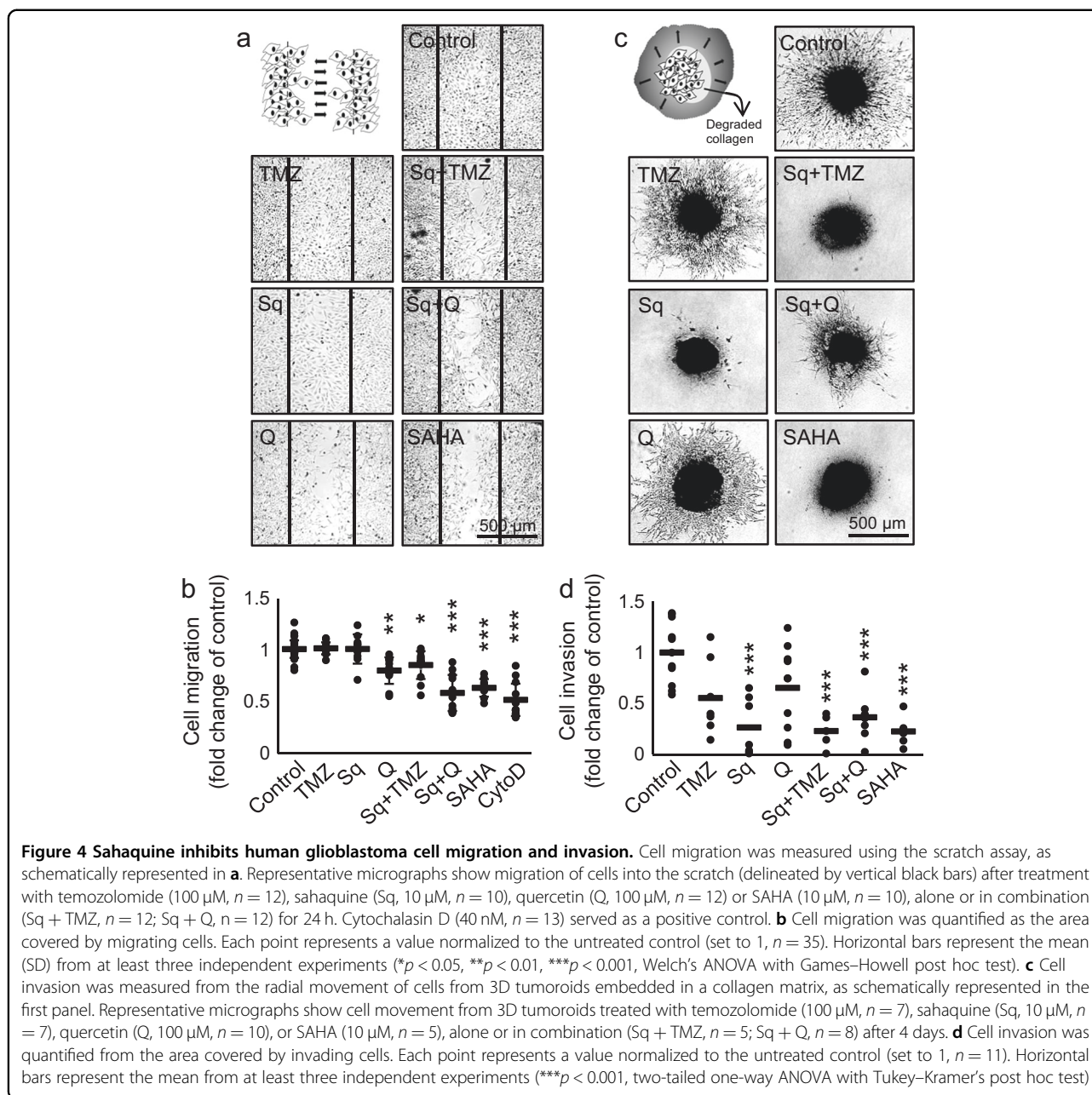
Sahaquine reduces EGFR abundance, ERK1/2, and AKT phosphorylation

EGFR overexpression and downstream hyperactivity of ERK1/2 and AKT are associated with worse prognosis in GBM^{39,40}. We assessed the abundance of these markers and HDAC6 in GBM by immunohistochemistry, and showed an increase in EGFR, dually phosphorylated (active) ERK1/2, phosphorylated (active) AKT, and HDAC6 compared to control brains (Fig. 6a). To test whether sahaquine impinges on EGFR and the activation of downstream kinases, we measured EGFR abundance, dual ERK1/2 phosphorylation (Thr202/Tyr204), and AKT phosphorylation (Ser473) by Western blotting (Fig. 6b). Sahaquine reduced EGFR concentrations in GBM. Interestingly, combining sahaquine and TMZ abrogated this inhibitory effect. Sahaquine also reduced levels of phosphorylated ERK1/2 and phosphorylated AKT, alone and in combination with quercetin or TMZ. Total ERK1/2 and AKT protein levels remained unchanged (Supplementary Fig. S8).

Discussion

Results from this study show that sahaquine is more effective than TMZ in killing glioblastoma and BTSCs, as well as inhibiting glioblastoma invasiveness. The mode of action of sahaquine implicates in part excessive α -tubulin acetylation due to the selective inhibition of HDAC6, resulting in cytoskeletal reorganization (Supplementary Fig. S9) and reduced invasiveness. Additional modes of action involve decreased EGFR abundance and downstream activity of AKT and ERK1/2. These results are particularly striking in combination with TMZ or quercetin.

TMZ is one of few clinically approved drugs for the treatment of GBM, but a substantial portion of newly diagnosed tumors and recurrent tumors are resistant to this drug^{3,41}. HDAC inhibitors are of particular interest for GBM treatment, as their effectiveness is unaltered by mechanisms of resistance upregulated in GBM, such as mismatch-repair, O⁶-methylguanine methyltransferase and base-excision repair^{3,4,42}. The pan-HDAC inhibitor SAHA is currently in clinical trials for GBM, but results so far showed marginal improvement in overall survival (5.7 months compared to



4.4 months) and several serious side effects^{6–9,43,44}. This and other current therapeutic interventions for GBM are ineffective^{28,29,31}.

Thus, our goal was to test a new hybrid compound. The development of hybrid molecules is one of the most active areas in therapeutics. Hybrid compounds can have multiple targets, reducing the risk of resistance, lowering effective doses, and decreasing side effects^{45,46}. Sahaquine is a hybrid molecule consisting of hydroxamic acid and primaquine linked by a dicarboxylic acid. Primaquine is a strong base (pI = 13.7), but addition of the hydroxamic acid group lowers its pI to 6.48, making sahaquine a weak

acid. Weak acids are more advantageous than weak bases as anticancer therapeutics, because they will not be protonated in the acidic tumor environment or trigger lysosomal exocytosis^{16–18}. Similarly to primaquine, sahaquine can also inhibit P-glycoprotein activity (Supplementary Fig. S6), thereby preventing multidrug resistance.

One of the great challenges in GBM treatment is heterogeneity, both within and between tumors^{47–50}. Inter-patient heterogeneity has been shown through genomic and transcriptomic analyses by the Cancer Genome Atlas research network^{51,52}. Intratumoral heterogeneity can be attributed to the different cellular lineages and subtypes

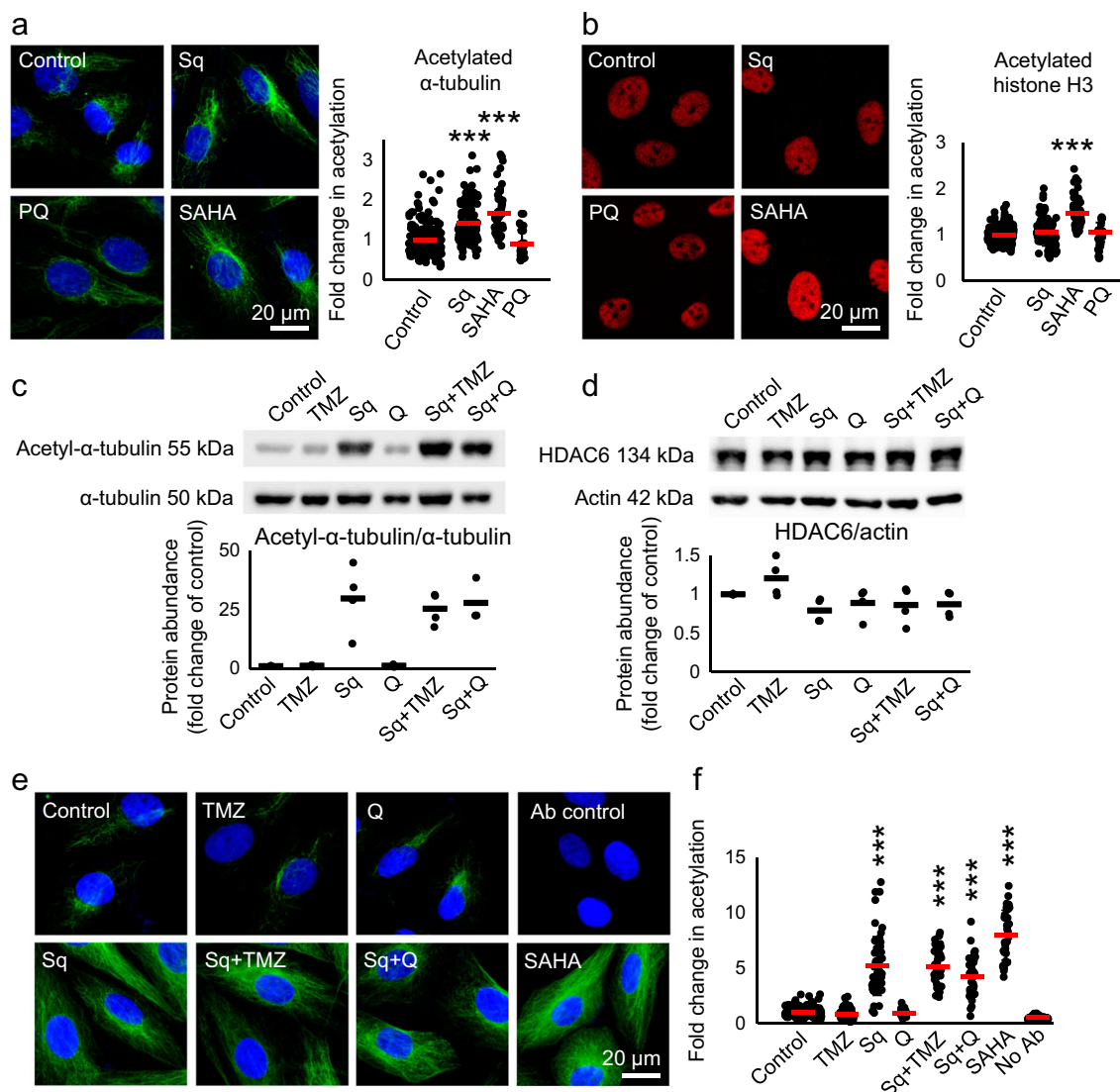


Figure 5 Sahaquinone-mediated HDAC6 inhibition results in selective α -tubulin hyperacetylation at nanomolar concentrations. **a**

Representative fluorescence micrographs of GBM α -tubulin acetylation (green) at lysine 40 in response to sahaquinone (Sq, 100 nM, $n = 121$ cells), SAHA (100 nM, $n = 54$ cells) or primaquine (PQ, 10 μ M, $n = 30$ cells) treatment for 24 h. **b** Representative fluorescence micrographs of GBM histone H3 acetylation (red) at lysine 9/lysine 14 in response to sahaquinone (Sq, 100 nM, $n = 120$ cells), SAHA (100 nM, $n = 90$ cells) or primaquine (PQ, 10 μ M, $n = 83$ cells) for 24 h. Nuclei (blue) were labeled with Hoechst 33342. Cells were imaged using a fluorescence microscope and fluorescence was analyzed in ImageJ. Shown are averages of fluorescence per cell (SD) normalized to the untreated controls (set to 1) from at least three independent experiments ($***p < 0.001$, Welch's ANOVA with Games–Howell post hoc test). **c** Acetylated α -tubulin ($n = 3$) and **d** HDAC6 protein abundance ($n = 4$) in GBM cells treated with temozolomide (TMZ, 100 μ M), sahaquinone (Sq, 10 μ M) or quercetin (Q, 100 μ M) alone or in combination for 24 h, measured by Western blotting. Acetylated α -tubulin and HDAC6 were normalized to total α -tubulin and actin, respectively. Each point represents a value normalized to the untreated control (set to 1). Horizontal bars represent the mean from at least three independent experiments. **e** Representative fluorescence micrographs of GBM α -tubulin acetylation (green) at lysine 40 in response to temozolomide (TMZ, 100 μ M, $n = 76$ cells), sahaquinone (Sq, 10 μ M, $n = 56$ cells), quercetin (Q, 100 μ M, $n = 32$ cells) or SAHA (10 μ M, $n = 36$ cells) alone or in combination for 24 h. Nuclei (blue) were labeled with Hoechst 33342. **f** Shown are averages (SD) of fluorescence per cell normalized to the untreated control (set to 1, $n = 197$ cells) from at least three independent experiments ($***p < 0.001$, Welch's ANOVA with Games–Howell post hoc test)

present in different parts of the same tumor^{53,54}, or even in individual cells within a tumor^{52,55}. Another cause of GBM heterogeneity is the presence of BTSCs, a subset of glioma cells with the abilities of self-renewal, differentiation, and recapitulation of the original tumor upon

xenotransplantation^{56–58}. They are resistant to radiation²⁸ and chemotherapy^{59–61}, and are thought to promote tumor recurrence^{30,31}. Therefore, effective GBM treatment demands a better understanding of tumor origin and heterogeneity to identify new therapeutic targets^{3,62}.

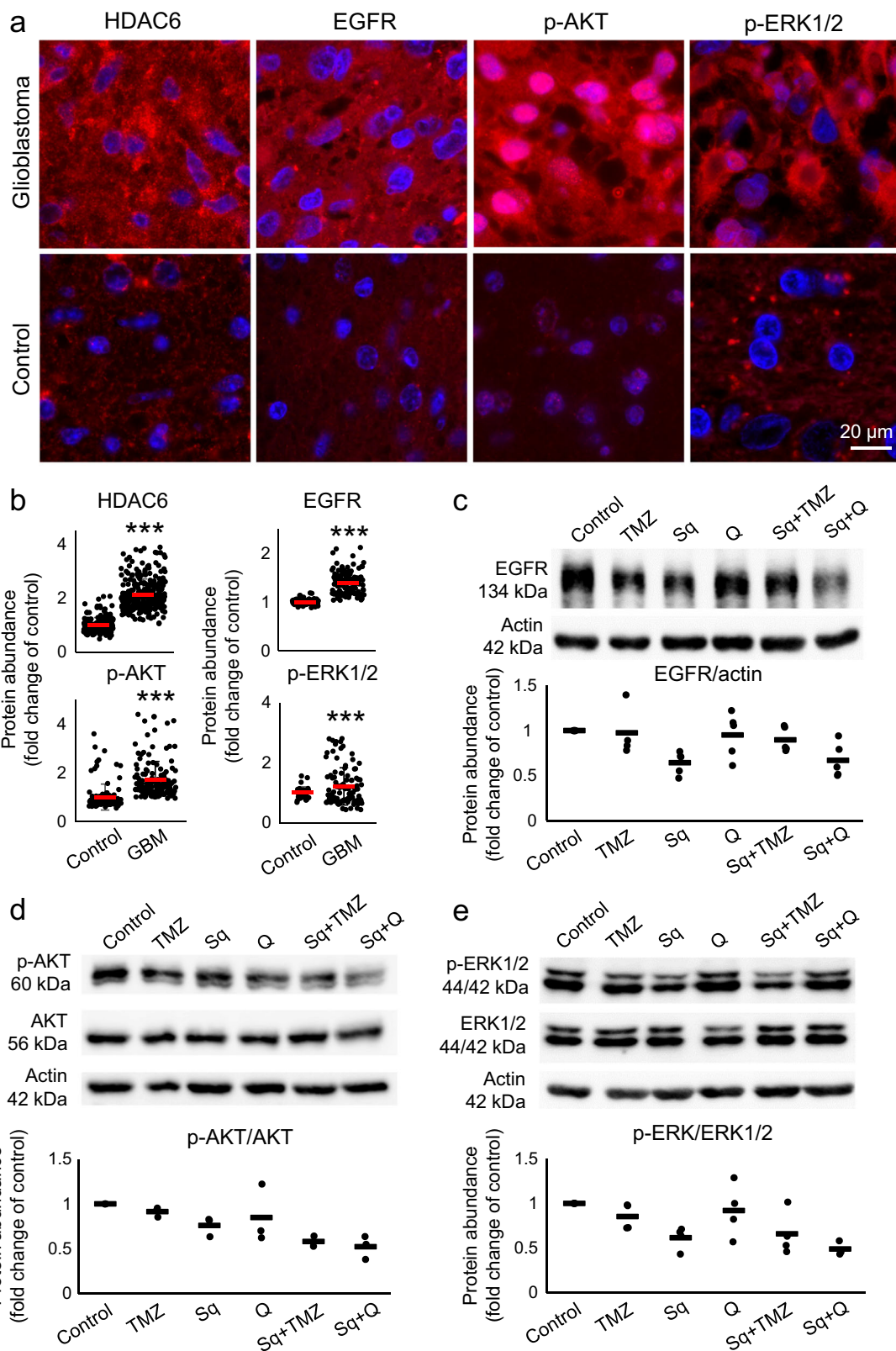


Figure 6 (See legend on next page.)

(see figure on previous page)

Figure 6 Sahaquine reduces EGFR abundance and AKT/ERK1/2 phosphorylation in human glioblastoma. **a** Representative fluorescence micrographs of human brain sections (GBM or healthy control) labeled for HDAC6, EGFR, phosphorylated AKT (p-AKT), or dually phosphorylated ERK1/2 (p-ERK1/2). Nuclei (blue) were labeled with Hoechst 33342. Cells were imaged using a fluorescence microscope and fluorescence was analyzed in ImageJ. **b** Horizontal bars represent averages of fluorescence per cell (SD) for HDAC6 (control, $n = 181$ cells, GBM, $n = 272$ cells), EGFR (control, $n = 94$ cells, GBM, $n = 116$ cells), p-AKT (control, $n = 115$ cells, GBM, $n = 147$ cells) and p-ERK1/2 (control, $n = 35$ cells, GBM, $n = 104$ cells). Each point represents a value normalized to the healthy control (set to 1) (** $p < 0.001$, Welch's ANOVA with Games–Howell post hoc test). **c** EGFR (TMZ, $n = 4$, Sq, $n = 5$, Q, $n = 5$, Sq + TMZ, $n = 5$, Sq + Q, $n = 5$), **d** phosphorylated AKT ($n = 3$), and **e** phosphorylated ERK1/2 (TMZ, $n = 4$, Sq, $n = 4$, Q, $n = 4$, Sq + TMZ, $n = 4$, Sq + Q, $n = 3$) protein abundances were measured in GBM cells treated with temozolomide (TMZ, 100 μ M), sahaquine (Sq, 10 μ M), or quercetin (Q, 100 μ M) alone or in combination for 24 h, by Western blotting. EGFR protein abundance was normalized to the actin loading control. Phosphorylated AKT and ERK1/2 were normalized to total AKT and total ERK1/2, respectively. Each point represents a value normalized to the untreated control (set to 1). Horizontal bars represent means from at least three independent experiments

Sahaquine (10 μ M) abolished the formation of BTSC neurospheres and significantly reduced the size of BTSC aggregates. TMZ was less effective, even at a tenfold higher concentration (100 μ M). Quercetin was as effective as sahaquine in killing BTSCs, but showed limited cytotoxicity toward differentiated GBM cells. Sahaquine eliminated both BTSCs and differentiated cancer cells.

Another factor contributing considerably to GBM recurrence is tumor invasiveness. While sahaquine abolished invasiveness and contributed to the loss of tumoroid viability, it did not markedly affect the abundance of secreted MMPs. In contrast, quercetin had limited effects on tumoroid viability, but decreased GBM invasion by inhibiting MMP secretion. Quercetin inhibits nuclear factor- κ B (NF- κ B) nuclear translocation, which could alter MMP expression^{63,64} and enhance cell death through NF- κ B-dependent regulation of apoptosis.

In an effort to reduce undesirable side effects in normal cells, selective HDAC inhibitors have been developed^{65,66}. Ricolinostat (ACY-1215) is a selective HDAC6 inhibitor currently in clinical trials (phase I and II) in combination with pomalidomide for multiple myeloma⁶⁷. Ricolinostat inhibits heat shock protein 90 deacetylation, resulting in an accumulation of unfolded proteins, disruption of protein homeostasis and cell death⁶⁸. We show that sahaquine selectively inhibits HDAC6 at nanomolar concentrations, which distinguishes it from SAHA, which is non-selective at equimolar concentrations. Interestingly, sahaquine significantly reduced the abundance of heat shock protein 70 in GBM (Supplementary Fig. S10) and altered α -tubulin organization. We have previously shown that celastrol disrupts protein homeostasis⁶⁹ and the organization of the F-actin cytoskeleton in GBM⁷⁰. Future studies will have to evaluate how sahaquine affects proteostasis in relation to cytoskeletal dynamics.

Many drugs currently in clinical trials aim at inhibiting proteins and proliferation pathways deregulated in GBM, notably HDAC6, EGFR, AKT, and ERK1/2^{71–74}. Our *in vitro* studies showing enhanced ERK1/2 and AKT phosphorylation are corroborated by immunohistochemical data in tumor sections from GBM patients (Fig. 6a),

also showing markedly stronger signals for HDAC6, EGFR, phosphorylated ERK1/2, and phosphorylated AKT compared to normal brain tissue (Fig. 6a). Sahaquine can decrease the abundance of EGFR, phosphorylated AKT, and phosphorylated ERK1/2 in GBM (Fig. 6b), thereby suggesting that similar hybrid molecules are viable candidates for GBM combination therapy. Interestingly, AKT deacetylation by HDAC6 promotes cancer growth and proliferation⁷⁵, indicating that sahaquine could reduce AKT activation through HDAC6 inhibition.

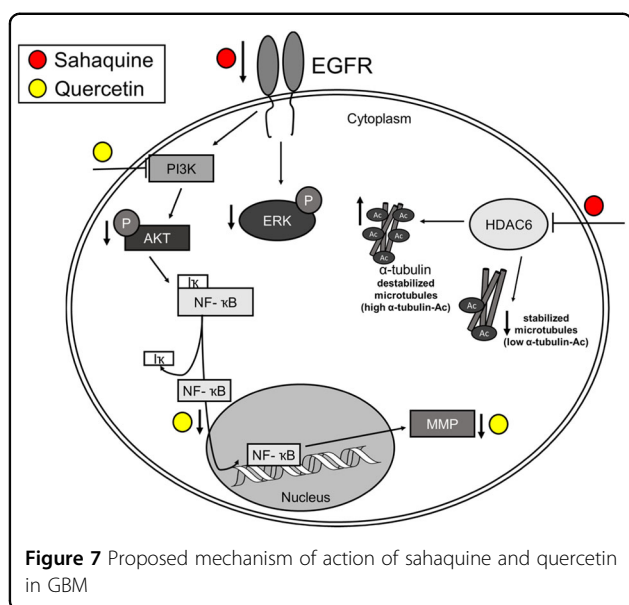
Drug resistance is a major problem in glioblastoma therapy^{3,41}. A recent study of HDAC inhibitors in drug-resistant melanoma implicated increased levels of reactive oxygen species⁷⁶. Combination of sahaquine with buthionine sulfoximine, which depletes endogenous glutathione levels⁷⁷, sensitized GBM cells to reactive oxygen species and enhanced cell death (Supplementary Fig. S11), although buthionine sulfoximine alone in the tested concentration had no effect on GBM viability. Further analysis of the effect of sahaquine on reactive oxygen species production in GBM is warranted.

Taken together, our study reveals sahaquine as a therapeutic agent affecting multiple cellular factors and processes that are critical for GBM treatment (Fig. 7). Sahaquine is superior to the clinical standard TMZ in reducing GBM and BTSC viability, invasiveness, and markers of key survival pathways. These effects are even more profound when sahaquine is combined with TMZ, buthionine sulfoximine, or quercetin. In conclusion, sahaquine is an effective cell death inducer which eliminates not only GBM cells but also BTSCs, thus suggesting that evaluation of sahaquine in combination with other drugs merit further investigations in patient-derived organoids, and eventually in humans.

Materials and methods

Synthesis of sahaquine

Sahaquine 5 was synthesized in four reaction steps (Fig. 1) adapted from the synthetic approach of Zhang et al.⁴⁵. Details of these steps are provided in the Supplementary Information. The first step included amide bond



formation between mono-methyl glutarate (**1**, Sigma-Aldrich, St. Louis, MO, USA) and primaquine (Sigma-Aldrich, St. Louis, MO, USA), with 1-[bis(dimethylamino)methylene]-1*H*-1,2,3-triazolo[4,5-*b*]pyridinium 3-oxid hexafluorophosphate (HATU, Alfa Aesar, Thermo Fisher, Kandel, Germany) as a coupling agent and *N,N*-diisopropylethylamine (DIEA, Alfa Aesar, Thermo Fisher, Kandel, Germany) as a base. The prepared product **2** was further hydrolyzed with lithium hydroxide (Sigma-Aldrich, St. Louis, MO, USA) and gave carboxylic acid **3**. In the next step, **3** was coupled with *O*-benzylhydroxylamine (Sigma-Aldrich, St. Louis, MO, USA) in the presence of HATU/DIEA and yielded *O*-benzylhydroxamic acid **4**, which was deprotected by catalytic hydrogenation and gave the target compound **5** (sahaquine). All reactions proceeded at room temperature.

Cell culture and tissue samples

U251N human glioblastoma cells were originally obtained from the American Type Culture Collection. Cells were cultured in Dulbecco's modified Eagle's media (DMEM, Gibco, Thermo Fisher Scientific, Grand Island, NY, USA) supplemented with 5% (v/v) fetal bovine serum (Wisent, St. Bruno, Canada) and 1% (v/v) penicillin–streptomycin (Thermo Fisher Scientific, Eugene, OR, USA) at 37 °C with 5% CO₂ and 95% relative humidity, unless otherwise indicated. Glioblastoma samples were harvested under a protocol approved by the Montreal Neurological Hospital's research ethics board (NEU-10-066). Consent was given by all patients. At least 116 brain sections from GBM patients aged 55–76 and controls were used. Tissues were from the frontal, temporal, or parietal lobes of the cerebral cortex. Human

BTSCs were expanded as neurospheres in complete NeuroCult™ proliferation media (Stemcell Technologies, Vancouver, BC, Canada). NeuroCult™ basal medium contained: NeuroCult™ NS-A proliferation supplement (1/10), recombinant human epidermal growth factor EGF (20 ng/ml), recombinant human basic fibroblast growth factor (20 ng/ml), and heparin (2 μg/ml).

Cell counting assay

U251N cells were seeded in 96-well black plates (Costar, Corning, NY, USA) at 5,000 cells per well in 0.1 ml media and cultured for 24 h. Cells were treated with sahaquine (0.001, 1, 5, 10, 20, 25, 30, 40, and 50 μM), TMZ (0.001, 1, 10, 50, 100, 200, 300, 400, and 500 μM, Sigma-Aldrich, St. Louis, MO, USA), quercetin (0.001, 1, 10, 25, 50, 75, 100, 200, and 300 μM, Sigma-Aldrich, St. Louis, MO, USA), or SAHA (0.001, 0.1, 1, 2, 5, 8, 10, 25, and 50 μM, Cayman Chemical, Ann Arbor, MI, USA) for 24 or 72 h. Combination treatments included increasing concentrations of sahaquine (0.001, 1, 3, 5, 7, 10, 20, and 50 μM) with quercetin (100 μM), increasing concentrations of quercetin (0.001, 1, 10, 25, 50, 100, and 200 μM) with sahaquine (10 μM), TMZ (30 μM) with sahaquine (10 μM), quercetin (140 μM) or SAHA (1 μM), and buthionine sulfoximine (100 μM, Sigma-Aldrich, St. Louis, MO, USA) with sahaquine (10 μM) for 24 h or 72 h. Following treatment, cells were fixed with 4% paraformaldehyde (w/v, 10 min, BDH, Toronto, ON, Canada). Nuclei were labeled with Hoechst 33342 (10 μM, 10 min, Thermo Fisher Scientific, Eugene, OR, USA). Cells were washed with phosphate-buffered saline and imaged using a fluorescence microscope (Leica DMI4000B, Toronto, ON, Canada).

BTSC viability

48EF human brain tumor cells were seeded at 5,000 cells per well in 96-well plates (Sarstedt, Nümbrecht, Germany) and treated for 7 days. Cells were then imaged using light microscopy (Leica DMI4000B) and the surface areas of the neurospheres were measured in ImageJ (version 1.51s).

Scratch assay

U251N cells were seeded in 6-well plates (Sarstedt, Nümbrecht, Germany) at 1,500,000 cells per well in 1 ml media and cultured for 24 h. The scratch was performed by gently dragging a 200 μl pipette tip across the cell monolayer, after which cells were washed with phosphate-buffered saline and incubated in DMEM with or without treatment. Cytochalasin D (40 nM, Sigma-Aldrich, St. Louis, MO, USA) served as positive control. Pre-determined areas of the wells were imaged using light microscopy immediately after the scratch (time = 0 h) and after 24 h. The cell-free area of the scratch was measured in ImageJ.

Cell invasion assay

U251N tumoroids were prepared using the hanging drop method⁷⁸. Drops of 30,000 cells in 20 μ l medium were pipetted onto the inner side of a 10 cm Petri dish (Thermo Fisher Scientific, Eugene, OR, USA) lid. The lid was quickly flipped to cover the Petri dish filled with 20 ml phosphate-buffered saline. Hanging drops were cultured at 37 °C for 48 h to allow tumoroids to form. Tumoroids were then gently scooped into a medium-filled Petri dish coated with 2% agarose and cultured for 48 h. Tumoroids were implanted in collagen gel (Advanced BioMatrix, San Diego, CA, USA) mixed with DMEM (1 \times) and sodium hydroxide (10 mM, Sigma-Aldrich, St. Louis, MO, USA). Gels were covered with 500 μ l DMEM with or without treatment. Tumoroids were imaged using light microscopy immediately after implantation (time = 0 day) and after 4 days. The area of cell invasion was measured in ImageJ.

Immunocytochemistry

Following treatment, U251N human glioblastoma cells were fixed with 4% paraformaldehyde (10 min), and then permeabilized using 0.1% Triton X-100 (v/v, 10 min, Sigma-Aldrich, St. Louis, MO, USA). Blocking was performed with 10% goat serum (v/v, 1 h, Thermo Fisher Scientific, Eugene, OR, USA) in phosphate-buffered saline, and then samples were incubated with primary antibodies (acetyl-histone H3 K9/K14, 1/500, Cell Signalling, #9677; acetyl- α -tubulin K40, 1/500, Santa Cruz, sc-23950; α -tubulin, 1/1000, Abcam, ab7291) overnight at 4 °C in a humidified chamber. Samples were washed three times with phosphate-buffered saline with 5 min incubation between washes. Secondary antibodies (anti-rabbit Alexa Fluor 488, 1/500, Thermo Fisher Scientific, A11008; anti-mouse Alexa Fluor 647, 1/500, Thermo Fisher Scientific, A28181) were incubated with samples for 1 h in the dark, and then washed off three times with phosphate-buffered saline with 5 min incubation in between washes. Nuclei were labeled with Hoechst 33342 (10 μ M, 10 min). Samples were mounted on microscope slides using Aqua-Poly/Mount (Polysciences, Warrington, PA, USA) and dried overnight before imaging with a fluorescence microscope (Leica DMI4000B).

Immunohistochemistry

Human brain sections were dewaxed in xylene, and then rehydrated in ethanol. Antigen retrieval was performed in citrate buffer using a decloaking chamber for 3 h. Samples were washed twice with double-distilled water, three times with phosphate-buffered saline, and then blocked with Protein Block (10 min, Spring Biosciences, Pleasanton, CA, USA). Samples were incubated with primary antibodies (HDAC6, 1/100, Santa Cruz, sc-11420; EGFR, 1/100, Oncogene Science Ab-1; phospho-AKT Ser473, Cell Signalling, #9271; phospho-p44/42 Erk1/2 Thr202/

Tyr204, 1/100, Cell Signalling, #9101) overnight at 4 °C in a humidified chamber. Samples were washed twice with IF buffer (0.05% (v/v) Tween 20, 0.2% (v/v) Triton X-100 in phosphate-buffered saline). Secondary antibodies (anti-rabbit Alexa Fluor 647, 1/500, Thermo Fisher Scientific, A21245; anti-rabbit Alexa Fluor 488, 1/1000, Thermo Fisher Scientific, A27034; anti-mouse Alexa Fluor 647, 1/1000, Thermo Fisher Scientific, A-21235) diluted in 2% (w/v) bovine serum albumin (Sigma-Aldrich, St. Louis, MO, USA) in phosphate-buffered saline were incubated with samples for 1 h in the dark at room temperature. Samples were washed three times with IF buffer, and then nuclei were labeled with DAPI (4',6-diamidino-2-phenylindole; 1 μ g/ml, 5 min, Molecular Probes, Eugene, OR, USA). Samples were washed three times with phosphate-buffered saline, then mounted on microscope slides using mounting media (Dako, Mississauga, ON, Canada), and air-dried for at least 30 min. Samples were imaged using a fluorescence microscope (Leica DMI4000B).

Western blotting

Western blot analysis followed published procedures⁷⁰. In brief, crude extracts were separated by sodium dodecyl sulfate–polyacrylamide gel electrophoresis (SDS-PAGE) and blotted onto nitrocellulose membranes. Blocked filters were probed with antibodies against acetyl- α -tubulin K40 (1/10,000, Sigma-Aldrich, St. Louis, MO, USA, #T7451), α -tubulin (1/1000, Santa Cruz, sc-5286), phospho-AKT Ser473 (1/2000, Santa Cruz, sc-7985), pan-AKT (1/1500, Cell Signaling, #9272), HDAC6 (1/1000, Santa Cruz, sc-11420), EGFR (1/1000, Santa Cruz, sc-03), phospho-ERK1/2 Thr202/Tyr204 (1/2000, Cell Signaling, #9106), pan-ERK1/2 (1/2000, Cell Signaling, #4695), and actin (1/100,000, Chemicon, MAB1501). Signals for enhanced chemiluminescence were acquired with a Bio-Rad ChemiDoc™ MP imaging system and quantified.

MTT assay

U251N cells were seeded in 24-well plates (Sarstedt, Nümbrecht, Germany) at 50,000 cells per well in 300 μ l media and cultured for 24 h. Cells were treated with sahaquine (0.001, 1, 5, 10, 25, and 50 μ M), TMZ (50, 100, 200, 300, 400, and 500 μ M), quercetin (10, 50, 100, and 200 μ M), or SAHA (0.1, 1, 2, 5, 8, 10, and 50 μ M) for 72 h. Combination treatments included increasing concentrations of sahaquine (1, 10, and 50 μ M) with a fixed concentration of quercetin (100 μ M), or increasing concentrations of quercetin (10, 100, and 200 μ M) with a fixed concentration of sahaquine (10 μ M) for 72 h. Following treatment, MTT (Sigma-Aldrich, St. Louis, MO, USA) dissolved in phosphate-buffered saline was added to cells (0.5 mg/ml) for 1 h at 37 °C. After MTT-containing media were removed, dimethyl sulfoxide (0.5 ml) was added to each well to lyse cells and dissolve formazan.

Wells were sampled in triplicate and the optical density was measured at 595 nm using a microplate reader (Asys UVM 340, Biochrom, Holliston, MA, USA).

Gelatin zymography

U251N cells were seeded in 60-mm tissue culture dishes (Thermo Fisher Scientific, Rochester, NY, USA) at 1,500,000 cells per dish in 3 ml media and cultured for 24 h. Cells were treated in serum-deprived DMEM for 24 h. Following treatment, culture media were collected and concentrated 15-fold using 30 kDa centrifugal filters (Millipore, Cork, Ireland) following the manufacturer's recommendations. Concentrated media were separated by SDS-PAGE using gelatin (0.1%, w/v) and acrylamide (7.5%, w/v) gels under non-reducing conditions. Gels were washed for 30 min in renaturing solution (2.5% (v/v) Triton X-100 in double-distilled water) and 30 min in developing buffer (50 mM Tris, pH 7.8; 1% (v/v) Triton X-100; 1 μ M ZnCl₂, 5 mM CaCl₂, adjusted to pH 7.45). Gels were then incubated in fresh developing buffer at 37 °C overnight. Gels were stained with 0.5% (w/v) Coomassie Blue G250 (Bio-Rad, Richmond, CA, USA) dissolved in 40% (v/v) ethanol and 10% (v/v) acetic acid for 1 h, and then destained in 40% ethanol and 10% acetic acid diluted in double-distilled water, until clear bands appeared. Quantification of MMP-9 and MMP-2 abundance (as band area) was done in ImageJ.

Tumoroid viability

U251N tumoroids were prepared using the liquid overlay system⁷⁹. The 96-well cell culture plates were coated with 75 μ l of 2% (w/v) agarose (Life Technologies, Gaithersburg, MD, USA) dissolved in serum-deprived DMEM. The agarose was cooled for 30 min, then cells were seeded at 5,000 cells per well in 200 μ l media, and cultured for 4 days before treatment. Cells were treated for 7 days, and then imaged using a microscope (Leica DMI4000B). The surface area of tumoroids was analyzed in ImageJ.

Calcein-AM uptake

U251N cells were seeded in 96-well black plates at 5,000 cells per well in 0.1 ml media and cultured for 24 h before treatment. Cyclosporine A (Calbiochem, Toronto, Canada) served as a positive control for the inhibition of P-glycoprotein. Following treatment, cells were incubated in phenol-free Hanks' balanced Salt solution containing calcein-AM (0.5 μ M, Thermo Fisher Scientific, Eugene, OR, USA) and propidium iodide (3 μ M, Sigma-Aldrich, St. Louis, MO, USA) for 30 min at 37 °C. The media were replaced with fresh Hanks' balanced salt solution and cells were imaged using a fluorescence microscope (Leica DMI4000B). Cells positively labeled with propidium iodide were excluded from the analysis.

Statistics

Experiments were performed independently at least three times. Unless otherwise indicated, data are shown as mean (SD). Normality of data distribution was assessed by the Shapiro–Wilk test. For sample sizes larger than 30, the Central Limit Theorem allows the assumption of normal distribution. Equality of variances was assessed by Levene's test. If the assumptions of normality and homogeneity of variance were met, two-tailed one-way analysis of variance (ANOVA) with Tukey–Kramer's post hoc test were performed. If homogeneity of variance was not observed, Welch's ANOVA with the Games–Howell post hoc test were used. A *p* value smaller than 0.05 was considered statistically significant: **p* < 0.05, ***p* < 0.01, and ****p* < 0.001.

Acknowledgements

We wish to thank J. Choi and E. Gran for their contribution to initial experiments related to this study. D.M. thanks the Canadian Institute for Health Research (MOP-119425) and the Natural Sciences and Engineering Council of Canada (RGPIN 04994-15). K.P. is grateful to the Brilliant Night Foundation, and B.Z. thanks the Croatian Science Foundation (IP-2014-09-1501) for financial support.

Authors' contributions

D.M. designed and coordinated the project. M.B., I.Z., and U.S. performed the experiments. M.B., I.Z., D.M., and U.S. analyzed and discussed the data. D.M., U.S., P.U.L., K.P., B.Z., and Z.R. contributed with reagents or clinical samples and discussion. M.B., I.Z., and D.M. wrote the manuscript with the help from the rest of the authors.

Author details

¹Department of Pharmacology and Therapeutics, McGill University, Montreal, QC, Canada. ²Faculty of Pharmacy and Biochemistry, University of Zagreb, Zagreb, Croatia. ³Department of Physiology, McGill University, Montreal, QC, Canada. ⁴Brain Tumour Research Centre, Montreal Neurological Institute and Hospital, Department of Neurology and Neurosurgery, McGill University, Montreal, QC, Canada

Conflict of interest

The authors declare that they have no conflict of interest.

Publisher's note

Springer Nature remains neutral with regard to jurisdictional claims in published maps and institutional affiliations.

The online version of this article (<https://doi.org/10.1038/s41420-018-0103-0>) contains supplementary material, which is available to authorized users.

Received: 16 July 2018 Revised: 10 August 2018 Accepted: 21 August 2018
Published online: 26 September 2018

References

1. Weller, M. et al. European Association for Neuro-Oncology (EANO) guideline on the diagnosis and treatment of adult astrocytic and oligodendroglial gliomas. *Lancet Oncol.* **18**, e315–e329 (2017).
2. Weller, M. et al. MGMT promoter methylation in malignant gliomas: ready for personalized medicine? *Nat. Rev. Neurol.* **6**, 39–51 (2010).
3. Hegi, M. E. et al. MGMT gene silencing and benefit from temozolomide in glioblastoma. *N. Engl. J. Med.* **352**, 997–1003 (2005).

4. Erasmus, H., Gobin, M., Niclou, S. & Van Dyck, E. DNA repair mechanisms and their clinical impact in glioblastoma. *Mutat. Res. Rev. Mutat. Res* **769**, 19–35 (2016).
5. Johnstone, R. W. Histone-deacetylase inhibitors: novel drugs for the treatment of cancer. *Nat. Rev. Drug Discov.* **1**, 287–299 (2002).
6. Galanis, E. et al. Phase II trial of vorinostat in recurrent glioblastoma multiforme: a north central cancer treatment group study. *J. Clin. Oncol.* **27**, 2052–2058 (2009).
7. Hummel, T. R. et al. A pediatric phase 1 trial of vorinostat and temozolomide in relapsed or refractory primary brain or spinal cord tumors: a Children's Oncology Group Phase 1 Consortium Study. *Pediatr. Blood Cancer* **60**, 1452–1457 (2013).
8. Lee, E. Q. et al. Phase I study of vorinostat in combination with temozolomide in patients with high-grade gliomas: North American Brain Tumor Consortium Study 04-03. *Clin. Cancer Res.* **18**, 6032–6039 (2012).
9. Vorinostat and Radiation Therapy Followed by Maintenance Therapy With Vorinostat in Treating Younger Patients With Newly Diagnosed Diffuse Intrinsic Pontine Glioma—Full Text View—ClinicalTrials.gov. <https://clinicaltrials.gov/ct2/show/NCT01189266> (accessed 31 May 2018).
10. Weathers, S.-P. & Gilbert, M. R. Advances in treating glioblastoma. *F1000Prime Rep.* **6**, 46 (2014).
11. Gluzak, M. A. & Seto, E. Histone deacetylases and cancer. *Oncogene* **26**, 5420–5432 (2007).
12. Lee, D. H., Ryu, H.-W., Won, H.-R. & Kwon, S. H. Advances in epigenetic glioblastoma therapy. *Oncotarget* **8**, 18577–18589 (2017).
13. Grant, S., Easley, C. & Kirkpatrick, P. Vorinostat. *Nat. Rev. Drug Discov.* **6**, 21–22 (2007).
14. Bertrand, S., Hélesbeux, J.-J., Larcher, G. & Duval, O. Hydroxamate, a key pharmacophore exhibiting a wide range of biological activities. *Mini Rev. Med. Chem.* **13**, 1311–1326 (2013).
15. Gialeli, C., Theocharis, A. D. & Karamanos, N. K. Roles of matrix metalloproteinases in cancer progression and their pharmacological targeting. *FEBS J.* **278**, 16–27 (2011).
16. Corbet, C. & Feron, O. Tumour acidosis: from the passenger to the driver's seat. *Nat. Rev. Cancer* **17**, 577–593 (2017).
17. Mahoney, B. P., Raghunand, N., Baggett, B. & Gillies, R. J. Tumor acidity, ion trapping and chemotherapeutics. I. Acid pH affects the distribution of chemotherapeutic agents in vitro. *Biochem. Pharmacol.* **66**, 1207–1218 (2003).
18. Zhitomirsky, B. & Assaraf, Y. G. Lysosomal accumulation of anticancer drugs triggers lysosomal exocytosis. *Oncotarget* **8**, 45117–45132 (2017).
19. van Weert, A. W., Geuze, H. J., Groothuis, B. & Stoorvogel, W. Primaquine interferes with membrane recycling from endosomes to the plasma membrane through a direct interaction with endosomes which does not involve neutralisation of endosomal pH nor osmotic swelling of endosomes. *Eur. J. Cell Biol.* **79**, 394–399 (2000).
20. Kim, J.-H., Choi, A.-R., Kim, Y. K. & Yoon, S. Co-treatment with the anti-malarial drugs mefloquine and primaquine highly sensitizes drug-resistant cancer cells by increasing P-gp inhibition. *Biochem. Biophys. Res. Commun.* **441**, 655–660 (2013).
21. Yang, Z. J., Chee, C. E., Huang, S. & Sinicrope, F. A. The role of autophagy in cancer: therapeutic implications. *Mol. Cancer Ther.* **10**, 1533–1541 (2011).
22. Andres S. et al. Safety aspects of the use of quercetin as a dietary supplement. *Mol. Nutr. Food Res.* **62**, <https://doi.org/10.1002/mnfr.201700447> (2018).
23. Srivastava, S. et al. Quercetin, a natural flavonoid interacts with DNA, arrests cell cycle and causes tumor regression by activating mitochondrial pathway of apoptosis. *Sci. Rep.* **6**, 24049 (2016).
24. Calgarotto, A. K. et al. Antitumor activities of Quercetin and Green Tea in xenografts of human leukemia HL60 cells. *Sci. Rep.* **8**, 3459 (2018).
25. Sun, S., Gong, F., Liu, P. & Miao, Q. Metformin combined with quercetin synergistically repressed prostate cancer cells via inhibition of VEGF/PI3K/Akt signaling pathway. *Gene* **654**, 50–57 (2018).
26. Zhang, X., Guo, Q., Chen, J. & Chen, Z. Quercetin enhances cisplatin sensitivity of human osteosarcoma cells by modulating microRNA-217-KRAS axis. *Mol. Cells* **38**, 638–642 (2015).
27. Zanini, C. et al. Inhibition of heat shock proteins (HSP) expression by quercetin and differential doxorubicin sensitization in neuroblastoma and Ewing's sarcoma cell lines. *J. Neurochem.* **103**, 1344–1354 (2007).
28. Bao, S. et al. Stem cell-like glioma cells promote tumor angiogenesis through vascular endothelial growth factor. *Cancer Res.* **66**, 7843–7848 (2006).
29. Chen, J., McKay, R. M. & Parada, L. F. Malignant glioma: lessons from genomics, mouse models, and stem cells. *Cell* **149**, 36–47 (2012).
30. Dagogo-Jack, I. & Shaw, A. T. Tumour heterogeneity and resistance to cancer therapies. *Nat. Rev. Clin. Oncol.* **15**, 81–94 (2018).
31. Johnson, B. E. et al. Mutational analysis reveals the origin and therapy-driven evolution of recurrent glioma. *Science* **343**, 189–193 (2014).
32. Chemicalize—Instant Cheminformatics Solutions. <https://chemicalize.com/> (accessed 31 May 2018).
33. Holland, E. C. Glioblastoma multiforme: the terminator. *Proc. Natl. Acad. Sci. USA* **97**, 6242–6244 (2000).
34. Nakada, M., Okada, Y. & Yamashita, J. The role of matrix metalloproteinases in glioma invasion. *Front Biosci.* **8**, e261–e269 (2003).
35. Alaseem A. et al. Matrix metalloproteinases: a challenging paradigm of cancer management. *Semin. Cancer Biol.* <https://doi.org/10.1016/j.semcancer.2017.11.008> (2017).
36. Jacobsen, J. A., Major Jourden, J. L., Miller, M. T. & Cohen, S. M. To bind zinc or not to bind zinc: an examination of innovative approaches to improved metalloproteinase inhibition. *Biochim. Biophys. Acta* **1803**, 72–94 (2010).
37. Bieliaskas, A. V. & Pflum, M. K. H. Isoform-selective histone deacetylase inhibitors. *Chem. Soc. Rev.* **37**, 1402–1413 (2008).
38. Schäfer, S. et al. Phenylalanine-containing hydroxamic acids as selective inhibitors of class IIb histone deacetylases (HDACs). *Bioorg. Med. Chem.* **16**, 2011–2033 (2008).
39. Sanchez-Vega, F. et al. Oncogenic signaling pathways in the Cancer Genome Atlas. *Cell* **173**, 321–337.e10 (2018).
40. Shinjima, N. et al. Prognostic value of epidermal growth factor receptor in patients with glioblastoma multiforme. *Cancer Res.* **63**, 6962–6970 (2003).
41. Lee, S. Y. Temozolomide resistance in glioblastoma multiforme. *Genes Dis.* **3**, 198–210 (2016).
42. Caporali, S. et al. DNA damage induced by temozolomide signals to both ATM and ATR: role of the mismatch repair system. *Mol. Pharmacol.* **66**, 478–491 (2004).
43. Yin, D. et al. Suberoylanilide hydroxamic acid, a histone deacetylase inhibitor: effects on gene expression and growth of glioma cells in vitro and in vivo. *Clin. Cancer Res.* **13**, 1045–1052 (2007).
44. Peters, K. B. et al. Phase III trial of vorinostat, bevacizumab, and daily temozolomide for recurrent malignant gliomas. *J. Neurooncol.* **137**, 349–356 (2018).
45. Zhang, X. et al. The discovery of colchicine-SAHA hybrids as a new class of antitumor agents. *Bioorg. Med. Chem.* **21**, 3240–3244 (2013).
46. Meunier, B. Hybrid molecules with a dual mode of action: dream or reality? *Acc. Chem. Res.* **41**, 69–77 (2008).
47. Cavalli, F. M. G. et al. Intertumoral heterogeneity within medulloblastoma subgroups. *Cancer Cell* **31**, 737–754.e6 (2017).
48. Hunter, K. W., Amin, R., Deasy, S., Ha, N.-H. & Wakefield, L. Genetic insights into the morass of metastatic heterogeneity. *Nat. Rev. Cancer* **18**, 211–223 (2018).
49. Meacham, C. E. & Morrison, S. J. Tumour heterogeneity and cancer cell plasticity. *Nature* **501**, 328–337 (2013).
50. Lin, C.-C. J. et al. Identification of diverse astrocyte populations and their malignant analogs. *Nat. Neurosci.* **20**, 396–405 (2017).
51. Cancer Genome Atlas Research Network. Comprehensive genomic characterization defines human glioblastoma genes and core pathways. *Nature* **455**, 1061–1068 (2008).
52. Verhaak, R. G. W. et al. An integrated genomic analysis identifies clinically relevant subtypes of glioblastoma characterized by abnormalities in PDGFRA, IDH1, EGFR and NF1. *Cancer Cell* **17**, 98 (2010).
53. Sottoriva, A. et al. Intratumor heterogeneity in human glioblastoma reflects cancer evolutionary dynamics. *Proc. Natl. Acad. Sci. USA* **110**, 4009–4014 (2013).
54. Morrissy, A. S. et al. Spatial heterogeneity in medulloblastoma. *Nat. Genet.* **49**, 780–788 (2017).
55. Patel, A. P. et al. Single-cell RNA-seq highlights intratumoral heterogeneity in primary glioblastoma. *Science* **344**, 1396–1401 (2014).
56. Galli, R. et al. Isolation and characterization of tumorigenic, stem-like neural precursors from human glioblastoma. *Cancer Res.* **64**, 7011–7021 (2004).
57. Lee, J. et al. Tumor stem cells derived from glioblastomas cultured in bFGF and EGF more closely mirror the phenotype and genotype of primary tumors than do serum-cultured cell lines. *Cancer Cell* **9**, 391–403 (2006).
58. Singh, S. K. et al. Identification of human brain tumour initiating cells. *Nature* **432**, 396–401 (2004).
59. Liu, G. et al. Analysis of gene expression and chemoresistance of CD133+ cancer stem cells in glioblastoma. *Mol. Cancer* **5**, 67 (2006).
60. Bleau, A.-M. et al. PTEN/PI3K/Akt pathway regulates the side population phenotype and ABCG2 activity in glioma tumor stem-like cells. *Cell Stem Cell* **4**, 226–235 (2009).

61. Chen S.-F. et al. Nonadhesive culture system as a model of rapid sphere formation with cancer stem cell properties. *PLoS ONE* **7**, <https://doi.org/10.1371/journal.pone.0031864> (2012).
62. Fouse, S. D., Nakamura, J. L., James, C. D., Chang, S. & Costello, J. F. Response of primary glioblastoma cells to therapy is patient specific and independent of cancer stem cell phenotype. *Neuro-Oncology* **16**, 361–371 (2014).
63. Bond, M., Chase, A. J., Baker, A. H. & Newby, A. C. Inhibition of transcription factor NF- κ B reduces matrix metalloproteinase-1, -3 and -9 production by vascular smooth muscle cells. *Cardiovasc. Res.* **50**, 556–565 (2001).
64. Soubannier, V. & Stifani, S. NF- κ B signalling in glioblastoma. *Biomedicines* **5**, <https://doi.org/10.3390/biomedicines5020029> (2017).
65. Lee, J.-H. et al. Development of a histone deacetylase 6 inhibitor and its biological effects. *Proc. Natl. Acad. Sci. USA* **110**, 15704–15709 (2013).
66. Santo, L. et al. Preclinical activity, pharmacodynamic, and pharmacokinetic properties of a selective HDAC6 inhibitor, ACY-1215, in combination with bortezomib in multiple myeloma. *Blood* **119**, 2579–2589 (2012).
67. ACY-1215 (Ricolinostat) in Combination With Pomalidomide and Low-dose Dex in Relapsed-and-Refractory Multiple Myeloma—Full Text View—ClinicalTrials.gov. <https://clinicaltrials.gov/ct2/show/NCT01997840> (accessed 31 May 2018).
68. Kekatpure, V. D., Dannenberg, A. J. & Subbaramaiah, K. HDAC6 modulates Hsp90 chaperone activity and regulates activation of aryl hydrocarbon receptor signaling. *J. Biol. Chem.* **284**, 7436–7445 (2009).
69. Boridy, S., Le, P. U., Petrecca, K. & Maysinger, D. Celastrol targets proteostasis and acts synergistically with a heat-shock protein 90 inhibitor to kill human glioblastoma cells. *Cell Death Dis.* **5**, e1216 (2014).
70. Maysinger, D., Moquin, A., Choi, J., Kodiha, M. & Stochaj, U. Gold nanourchins and celastrol reorganize the nucleo- and cytoskeleton of glioblastoma cells. *Nanoscale* **10**, 1716–1726 (2018).
71. Combs, S. E. et al. Treatment of primary glioblastoma multiforme with cetuximab, radiotherapy and temozolomide (GERT)—phase I/II trial: study protocol. *BMC Cancer* **6**, 133 (2006).
72. Emrich, J. G. et al. Radioiodinated (I-125) monoclonal antibody 425 in the treatment of high grade glioma patients: ten-year synopsis of a novel treatment. *Am. J. Clin. Oncol.* **25**, 541–546 (2002).
73. Quang, T. S. & Brady, L. W. Radioimmunotherapy as a novel treatment regimen: ¹²⁵I-labeled monoclonal antibody 425 in the treatment of high-grade brain gliomas. *Int. J. Radiat. Oncol. Biol. Phys.* **58**, 972–975 (2004).
74. ONC201 in Adults With Recurrent H3 K27M-mutant Glioma—Full Text View—ClinicalTrials.gov. <https://clinicaltrials.gov/ct2/show/NCT03295396> (accessed 31 May 2018).
75. Iaconelli, J. et al. Lysine deacetylation by HDAC6 regulates the kinase activity of AKT in human neural progenitor cells. *ACS Chem. Biol.* **12**, 2139–2148 (2017).
76. Wang, L. et al. An acquired vulnerability of drug-resistant melanoma with therapeutic potential. *Cell* **173**, 1413–1425.e14 (2018).
77. Du, M., Zhang, L., Scorsone, K. A., Woodfield, S. E. & Zage, P. E. Nifurtimox is effective against neural tumor cells and is synergistic with buthionine sulfoximine. *Sci. Rep.* **6**, <https://doi.org/10.1038/srep27458> (2016).
78. Werbowetski-Ogilvie, T. et al. Inhibition of medulloblastoma cell invasion by Slit. *Oncogene* **25**, 5103–5112 (2006).
79. Dhanikula, R. S., Argaw, A., Bouchard, J.-F. & Hildgen, P. Methotrexate loaded polyether-copolyester dendrimers for the treatment of gliomas: enhanced efficacy and intratumoral transport capability. *Mol. Pharm.* **5**, 105–116 (2008).